Characterization and modeling of PPy bilayer microactuators Part 1. Curvature

Marc Christophersen [a], Benjamin Shapiro [b], Elisabeth Smela [a,*]

[a] *Mechanical Engineering Department, University of Maryland, College Park, MD 20742, USA*
[b] *Aerospace Engineering Department, University of Maryland, College Park, MD 20742, USA*

Abstract

Bilayer actuators of gold and polypyrrole doped with dodecylbenzenesulfonate, PPy(DBS), were microfabricated with lengths and thicknesses that varied over two orders of magnitude. The actuators were connected to rigid plates. The curvature of the bilayers was examined as a function of PPy and Au layer thicknesses to enable a determination of the actuation strain and Young's modulus of the PPy(DBS). Four different Au thicknesses were tested, and maximum curvature was obtained in all cases at a PPy:Au thickness ratio of 5:1. The data could not be fit with a constant value for the actuation strain; in addition, the PPy film bent even in the absence of an Au layer. Therefore, a model was developed that included strain and modulus variations along the direction of film thickness. The experimental data were fit with an exponential variation in actuation strain, starting at 20% at the surface of the PPy and decreasing to 3% at the gold interface in thicker films. The Young's modulus was found to be constant between 0.08 and 0.20 GPa in the oxidized state. These values differ significantly from thick-film values. With this information, micro-actuators can now be designed to achieve a specified radius of curvature.
© 2005 Elsevier B.V. All rights reserved.

Keywords: Micro-actuator; Polypyrrole; Bilayer; Curvature; Strain; Young's modulus

1. Introduction

Conjugated polymer actuation was first demonstrated in the early 1990s, and many proof-of-concept devices have been demonstrated since then. The technology is now in the early stages of commercialization. Therefore, research efforts have begun to focus on two areas: obtaining material properties and performance metrics (see for example [1]) and developing predictive models for actuator behavior so that systems utilizing conjugated polymer actuators can be designed and optimized. These advances in knowledge will allow end-users to evaluate the suitability of these "artificial muscles" for a given application, to compare their performance with other actuators, to utilize them in more complex systems, to understand the trade-offs between the various performance metrics, and to develop algorithms that control system dynamics. This paper on the curvature of microfabricated PPy/Au bilayer actuators is a contribution to this larger effort.

Bilayers have been the most commonly investigated actuator configuration, and they are of particular utility on the micro-scale [2]. Therefore, in Part 1 of this series we focus on bilayer curvature, in Part 2 on force, and in Part 3 on speed, the three metrics that are of primary importance for any actuator.

As a model system we chose polypyrrole doped with dodecylbenzenesulfonate, PPy(DBS), which we have used for all of our previous micro-actuator work (see for example [2] and references therein). DBS is a surfactant molecule consisting of a branched alkyl chain attached to a phenyl ring with a sulfonate group [3]. PPy(DBS) is a cation-transporting material that expands upon reduction and contracts upon oxidation. During the first reduction cycle, the bilayers remain flat on the surface. (Although the PPy expands substantially out of plane, it does not do so inplane, and bilayer curvature is controlled by inplane strain [3,4].) During the first oxidation cycle, the PPy contracts inplane, and the bilayers lift off the surface, bending PPy-side in. The bilayers reach their steady-state behavior after a few cycles. (Hysteresis upon changing cycling conditions

due to polymer chain conformational changes has been studied extensively by Otero et al. [5–7], and is not addressed in the present study.) The specific results in this paper are particular to PPy(DBS), but the general findings and approaches are applicable to other conjugated polymers, as well as to macro-scale bilayers and other types of elelectroactive polymer (EAP) actuators.

Timoshenko's classical model for metal bilayers that bend upon heating due to different coefficients of thermal expansion [8] provided a starting point for our analysis of actuator curvature. In 1992, Pei and Inganäs applied the Timoshenko equation to PPy/polyimide bilayers, backing out estimates of actuation strain [9–11]. This model assumes a constant strain in the material and requires a knowledge of the Young's moduli of the bilayer materials and their thicknesses. However, polypyrrole properties such as Young's modulus have only been obtained for thick films (10 μm or greater). Attempts to use this model for microactuators found that the assumption of constant actuation strain (i.e. constant strain coefficient α) throughout the PPy thickness was inconsistent with the bending angle data for micro-scale bilayers [12]. In addition, it was impossible to use a single set of modulus and strain values to predict bending in both macro- and micro-actuators made under the same conditions but varying in thickness.

The reason for the failure of this simple model lies in the non-uniform molecular structure and morphology of the PPy throughout its thickness as a consequence of electrochemical deposition. (In fact, virtually no conjugated polymer deposition method yields films with uniform properties along the out-of-plane z-axis. For instance, cast films have a variety of internal structures on the nano- and micro-scale that change from the substrate to the surface.) The material closer to the electrode is subjected to the polymerization voltage or current longer than the material at the electrolyte interface. This voltage can induce continued cross-linking, substitutions onto the backbone, or chain scission reactions, producing a higher electronic defect density. Defects reduce electroactivity, and thus the requirement for charge-compensating cations, leading directly to a decrease in strain. There may also be a change in modulus, depending on the type of defect: crosslinking would raise the modulus (and further hinder ion transport), substituents may not affect modulus substantially, and chain scission would lower the modulus.

There are several pieces of evidence for anisotropy along z in PPy(DBS). For example, PPy films that have delaminated from the Au electrode curl away from the substrate upon oxidation [12]. If the properties of PPy were constant in z, then the beam would not bend on its own. As another example, the resonant resistance in quartz crystal microbalance measurements during electrochemical deposition has been shown to undergo a sudden increase at a charge density of 60 mC/cm^2 (corresponding to a thickness of 0.3 μm), and this change in resonant resistance is associated with a change in viscoelastic properties [13]. Atomic force microscopy images of the same films suggest that the morphology of the polymer changes at that point: the initial material is laid down under a nucleation and growth mechanism, but once the nuclei coalesce, they grow upward into columns. As a final
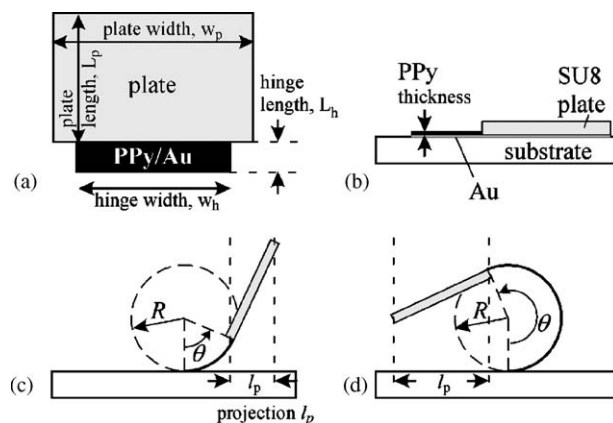

Fig. 1. Definition of dimensions, radius of curvature R, and bending angle θ for the actuators, which consisted of PPy/Au bilayers (hinges) and SU8 plates. Figure components are not to scale. The bending angles were determined from the vertical projection of the plate area, l_p/L_p.

example, out-of-plane strain is not constant with film thickness, but is greatest for films 1 μm thick [14].

The dependence of material properties and actuation metrics on film thickness makes rational design of micro-actuators impossible until the dependence is characterized quantitatively; otherwise one must rely on empirical trail and error. The applications being pursued in our laboratory include lidded vials for cell-based sensing and microvalves for treatment of urinary incontinence. The former must be designed to achieve specific bending angles, while the latter must overcome a given force, and in both cases the surface area occupied by the actuator is limited. In order to design such microactuators, it is necessary to understand the relationships between the bilayer geometric parameters (length, width, PPy thickness, and PPy to Au thickness ratio) and the resulting performance (radius of curvature and moment). Fig. 1 illustrates the dimensions and curvature parameters for the bilayers used in this study.

2. Experimental

2.1. Actuator design

Actuators were designed as shown in Fig. 1a and b. The "hinges" were PPy/Au bilayer bending beams, and the rigid plates were made of SU8, a negative photoresist. The plate, which was also backed by the Au layer, aided in visualizing the bending angle, as explained below.

Approximately 2500 devices were produced on each substrate. Bilayers were arranged in sets that were repeated 40 times over the surface. Each set comprised a wide range of hinge lengths: 4, 6, 8, 10, 15, 20, 30, 50, 75, 100, 125, 150, and 200 μm. There were four actuators of every hinge length per set, grouped together. The duplication allowed us to examine the uniformity of our fabrication process across the substrate and the reproducibility of the results. The samples were diced after fabrication so that sets of devices could be measured independently at different times, by different individuals, and under different conditions.

Our aim was to fabricate actuators with a wide range of PPy:Au thickness ratios as well as actuators with the same ratios but different total thicknesses. The former was accomplished by fabricating many identical sample substrates, and coating each with a different PPy thickness. The latter was achieved by producing the same range of ratios with different Au thicknesses (500, 1000, 2000, and 3000 Å of Au for a total of 28 different thickness combinations). (See the Supplementary Data for a table with details.)

The width of the hinges scaled with their length by a factor of 4:1, but for the shortest hinges (4, 6, 8, 10, and 15 μm) it was fixed at 50 μm. The length of the SU8 plate was kept constant at 150 μm, and the width of the plate was scaled with the hinge width by a factor of 1.025.

The wide range of hinge lengths ensured that measurable bending angles would be produced on every sample. The shortest hinges were needed for thin bilayers that had the optimal PPy:Au thickness ratio, which bent the most, while the longest hinges were needed for thick bilayers far from the optimal ratio, which bent the least.

2.2. Sample fabrication

The bilayers were fabricated by surface micromachining on oxidized (1 μm thermal oxide) (1 0 0)-oriented silicon wafers that had been cleaved into quarters. The process made use of differential adhesion, and was based on previously published work [3] with two modifications. First, SU8 was used as the rigid plate material instead of BCB. Second, the photoresist (Shipley, 1818) remaining after the last etching step was removed with ethanol rather than by reactive ion etching (RIE) to reduce the risk of damaging the structures by over-etching.

A high resolution Cr/glass mask (PhotoPlot Store) was used for the photolithography. The mask aligner (Karl Suss MJB3) had a 2 μm resolution and a 2 μm alignment accuracy.

The adhesion layer consisted of 40 Å of Cr (thermally evaporated at a rate of 1 Å/s at 5×10^{-6} Torr) topped by 300 Å of Au (5.0 Å/s, 5×10^{-6} Torr). The metals were patterned by wet chemical etching (etchants from Transene Company, Inc.) to open windows into the adhesion layer down to the oxide. A structural gold layer was deposited next (same conditions) to varying thicknesses; this film became the gold layer of the actuator. All thicknesses were measured by mechanical profilometry (Tencor AlphaStep500 or Veeco Dektak3030).

SU8-5 (MicroChem) was stored at 4 °C and warmed up to room temperature before use. During spin-coating, the speed was ramped from 0 to 500 rpm during the first 10 s, then up to 3000 rpm over the next 20 s. A soft bake was performed on a programmable hotplate that ramped the temperature to 95 °C at a rate of 300 °C/h. The sample was held for 5 min at 95 °C, then cooled back to room temperature over 30 min. The SU8 was exposed to light of 365 nm with a dose of 318 mJ/cm^2. A hard bake was done that was identical to the soft bake. The SU8 was developed for 3 min in SU8 developer (MicroChem), resulting in plates with a thickness of 5.1 μm.

PPy was deposited electrochemically (EcoChemie pgstat30) at 0.48 V versus Ag/AgCl (BAS) from an aqueous solution of 0.1 M NaDBS (Aldrich) and 0.1 M pyrrole (Aldrich). It was patterned by RIE in an oxygen plasma using a masking layer of photoresist (Shipley, 1818) 2 μm thick. The final steps were etching the structural Au to free the actuators and removing the resist in ethanol. The plates lifted slightly after immersion in ethanol, showing complete release from the substrate. The process sequence yielded between 90 and 100% working devices.

The dimensions used for the bilayers in this study represented the limits of what could be fabricated using this process sequence and equipment. Hinge dimensions were limited by three factors: alignment and resolution during photolithography and plasma etching. The former limited the minimum hinge length to 4 μm, and misalignment was a noticeable source of error in the shortest bilayers. The oxygen plasma etch selectivity (ratio of etch rates) between PPy and the masking 2 μm thick photoresist was 2.5:1, which placed an upper limit on the PPy thickness of 5 μm. Finally, the thinnest Au layer that could be used was fixed by the smallest hinge length, since if the Au were thinner, bilayers with the optimal PPy:Au thickness ratio would bend 180° in less than 4 μm, giving no curvature data (allowing only a lower limit of curvature to be estimated).

Some devices included a 500 Å thick electroplated Au film over the structural Au to promote adhesion with the PPy. The plating bath (Oromerse SO part B, Technic) was diluted 10:1 with NaSO$_3$. The deposition was performed potentiostatically at −0.9 V versus Ag/AgCl.

2.3. Bilayer actuation

All actuation experiments were performed in 0.1 M NaDBS. The samples were placed face-up and flat in a custom-fabricated electrochemical cell, held against the bottom with a gold-plated screw and nut (for a similar cell, see [4]). A graphite plate (VWR) was used as the counter electrode, and the Ag/AgCl reference electrode was placed as close as possible to the working electrode sample without touching it.

The hinges bent slightly upon immersion in the electrolyte for the first time. To ensure steady-state behavior before starting the measurements, the actuators were cycled 20 times at 50 mV/s between 0 and −1 V, corresponding to the fully oxidized and reduced states of the polymer. The bending of all the hinges was completely synchronized after five to eight cycles.

To record the bending angles, the potential was held at 0 V and then −1 V for approximately 30 min, the time it took to complete the entire wafer. Previously measured bilayers were spot-checked at the end to ensure that the angles had not changed over this time interval; they had not.

2.4. Data collection and analysis

Actuators were viewed from directly overhead using a Leica Z16 APO stereomicroscope with a 187 mm working distance. The aperture was closed to increase the depth of focus. Coaxial illumination was used, which is necessary for mirror-like surfaces. The light source was a 150 W tungsten halogen lamp (Schott-Fostec).
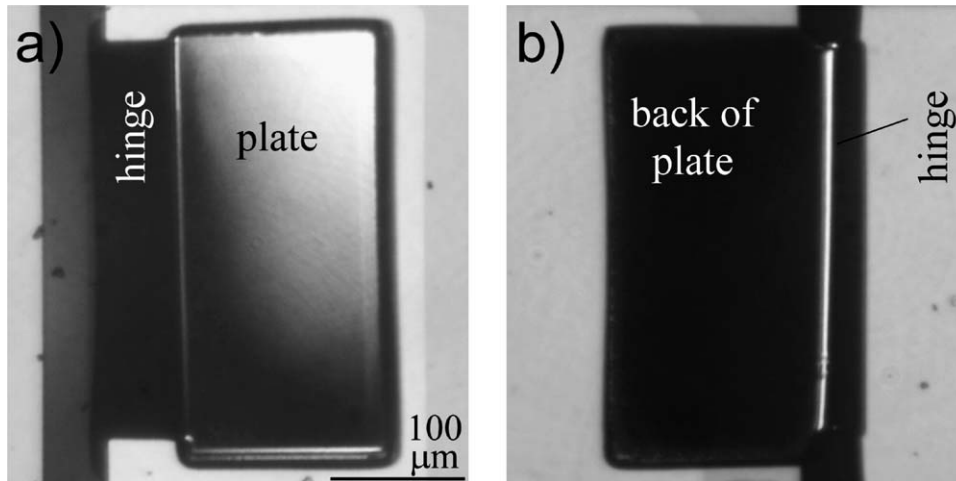
Fig. 2. Overhead photographs of a 50 µm long hinge with a 150 µm long plate in the (a) flat, reduced state and (b) bent, oxidized state, where the plate has rotated just over 180° and touched the substrate (the PPy:Au ratio was 9:1).

The bending angle of each flap in the fully oxidized and reduced states was determined from photographs taken through the microscope with a digital camera (Nikon Coolpix 3500, 2 MP, attached with a c-mount adapter). Bending angles were defined with respect to the silicon surface. In the reduced state, the bilayers laid flat at bending angles near zero.

The digital images were analyzed to determine the rotation of the flap using a projection method. The apparent length of the plate viewed from above (measured using the ruler function in the software package Designer) was compared to its length lying flat (Fig. 1), as well as to the width of the unvarying electrical interconnect lines. Geometrical relationships were used to determine the bending angle θ.

The largest source of error in determining bending angle was caused by incomplete removal, during RIE, of PPy around the outside edges of the SU8 plates. This excess PPy resulted in indistinct plate edges. Plate lengths were accurate to within 2 µm except when the plates were perpendicular to the surface, when shadowing reduced the accuracy to 5 µm. Photographs of a bilayer in the reduced and oxidized states, bent to 0° and >180°, respectively, are shown in Fig. 2. In this pair of images, the edges are crisp.

3. Results

3.1. Bending angle versus hinge length

The bending angles from four sets of devices are plotted as a function of hinge length in Fig. 3. Every point represents the bending angles of 16 identical hinges. Differences among hinges were less than a degree, so the error bars cannot be seen on this scale.

The bending angle increased linearly with hinge length, showing that there is a single radius of curvature R for all the devices on the wafer, which is evidence for a circular arc hinge shape (Fig. 1c and d). Above a particular threshold length, the

plate touches the surface, the hinge cannot bend further, and the curve flattens.

The PPy was slightly thicker where it touched the SU8 than it was elsewhere on the hinge. In the case of very short hinges, this led to increased or decreased bending angles, depending on the PPy:Au ratio.

3.2. Curvature versus PPy:Au ratio

Curvature $\kappa = 1/R$ was calculated for every point below the threshold length in the bending angle versus hinge length plots, and the values for each sample were averaged. Curvatures obtained from all the wafers are plotted versus PPy:Au thickness ratio in Fig. 4. Each point in Fig. 4 represents a minimum of six points from a curve such as Fig. 3, and the error bars are the standard deviations of the averaged values. (Curvature was mea-
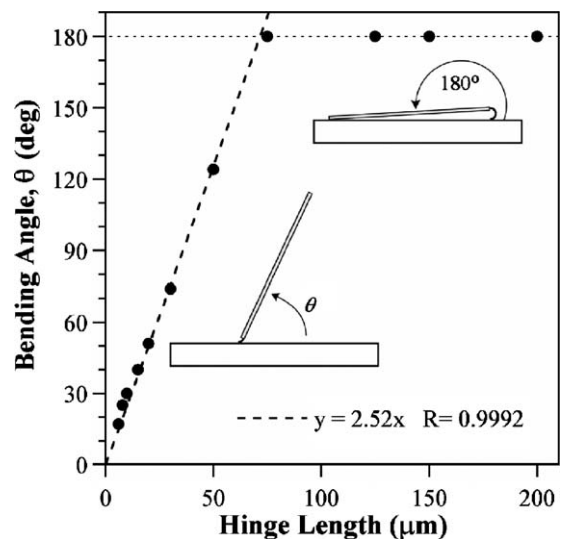

Fig. 3. Bending angle θ as a function of hinge length. The relationship is linear up to $L_h = 75$ µm, when the plate touches the substrate (as in Fig. 2b) (PPy:Au = 19:1, Au = 1000 Å).
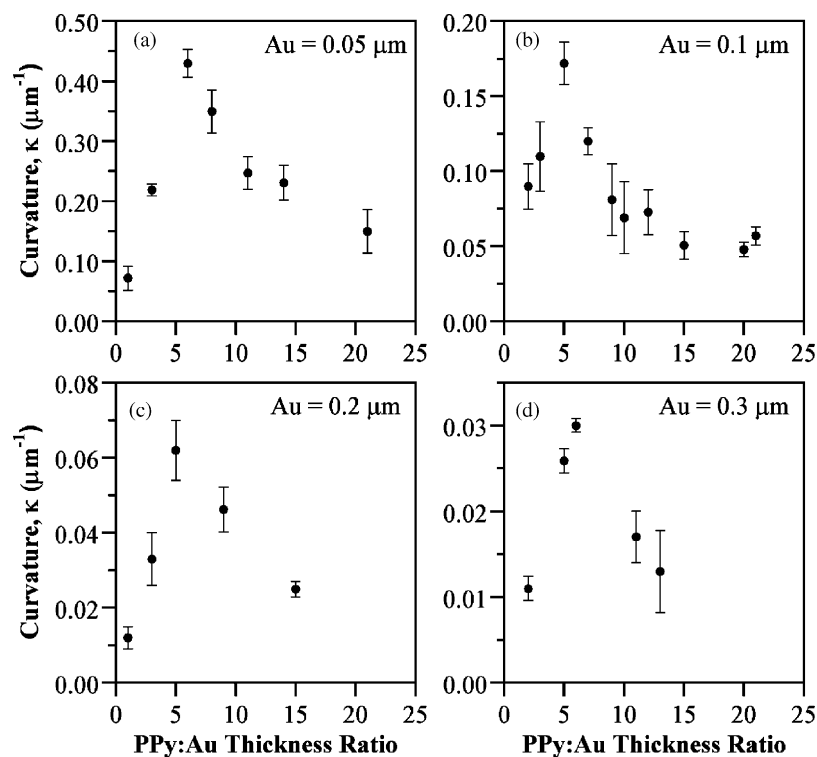
Fig. 4. Curvature as a function of PPy:Au thickness ratio for four different Au thicknesses.

sured independently by two different people for samples with 500, 1000, and 2000 Å gold thickness, and their data agreed. See the Supplementary Data for plots showing both sets of data.)

For each Au thickness, the data show a peak, as expected from the Timoshenko equation, and the peak occurs at the same thickness ratio of approximately 5:1 for all four Au thicknesses. The left–right position of the peak, as will be discussed further below, depends on the ratio of the Young's moduli of the two layers. The height depends on the actuation strain, the total bilayer thickness, the ratio of the thicknesses of the two layers, and the ratio of their Young's moduli.

The greatest curvature that was achieved was 0.5 μm^{-1} for Au layers 500 Å thick. This corresponds to a radius of curvature of only 2 μm. The smallest curvature was 0.01 μm^{-1} for Au layers 3000 Å thick at PPy:Au ratios far from the peak, which corresponds to a radius of 100 μm. (It should be noted that even this large radius is quite small compared to what can be achieved in micro-scale actuators made from inorganic materials, as well as in macro-scale PPy actuators.)

3.3. Curvature with electroplated Au

The PPy should not delaminate during actuation but should adhere strongly to the underlying Au layer. Adding a layer of electroplated gold over the smooth Au structural layer prior to PPy deposition improves adhesion by promoting mechanical inter-locking of the two materials, thus increasing actuator strain, force, and lifetime [15,16]. However, since the electroplated layer is not solid but rather nodular, it is unclear how

it behaves mechanically. The effective plated film thickness, which controls the curvature, must be related to the measured film thickness. We therefore fabricated two wafer quarters with 500 Å of plated Au over 1000 Å of evaporated Au.

The curvature data for these bilayers are shown in Fig. 5. The values lie between the 1000 and 2000 Å evaporated Au curves, but closer to the 1000 Å. Fitting these points using the model that best described our data (see Section 5), the 500 Å of plated Au behaved as if it had a thickness of approximately 300 Å.
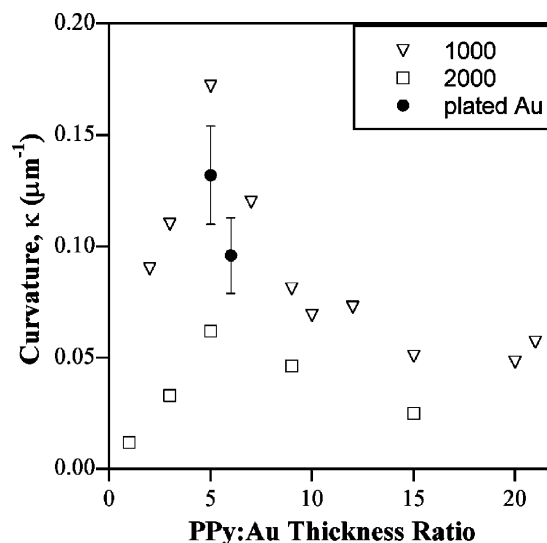

Fig. 5. Curvature vs. PPy:Au thickness ratio for bilayers with 500 Å of Au electroplated over 1000 Å of evaporated Au. The rough plated layer behaves equivalently to a solid Au film with a thickness of 300 Å.

3.4. Confirmation of method validity

Some of the actuators were designed without plates, and these were able to bend greater than 180°, even into spirals. Due to an error in the mask for some of these devices, a hole was etched through the bilayer. Fig. 6 shows a curled bilayer with the hole visible at the top. Since the position of this feature on the mask was known to be 275 μm from the hinge anchor point, images of such structures could be used as an independent method to determine curvature. They also allowed us to check whether bilayers with and without plates bent to the same radius.

The curvature for this sample was 0.0114 μm^{-1}. Fig. 7 shows this curvature in comparison with curvature data obtained by the projection method for hinges with the same Au thickness but with SU8 plates. The good agreement confirms that the bilayers bend into perfect circles and that the presence of the plates does not change the curvature.

4. Model

4.1. Model formulation

Classical beam theory was used to develop a model for bilayer bending and force (the latter is the focus of Part 2 of this series). The model has five assumptions:

1. The beam thickness h is small compared to the radius of curvature: $h \ll R$, where R is the radius of curvature measured to the polymer/gold interface.
2. The strain throughout a bent bilayer is determined only geometrically by the curvature (Fig. 1).
3. The relationship between stress and strain is linear, given by the Young's modulus, although the modulus may have a spatial dependence.
4. Strains and stresses are isotropic in the x- and y-directions.
5. The curvature along the width of the hinge can be neglected, and deflection is only a function of length.

The first assumption is valid for most of our samples, since $R/h > 10$ for all except three, which are thin and have PPy:Au ratios that yield maximum curvature ($R/h = 5.7$ for Au = 0.05 μm, PPy:Au = 6; $R/h = 8.2$ for Au = 0.05 μm,
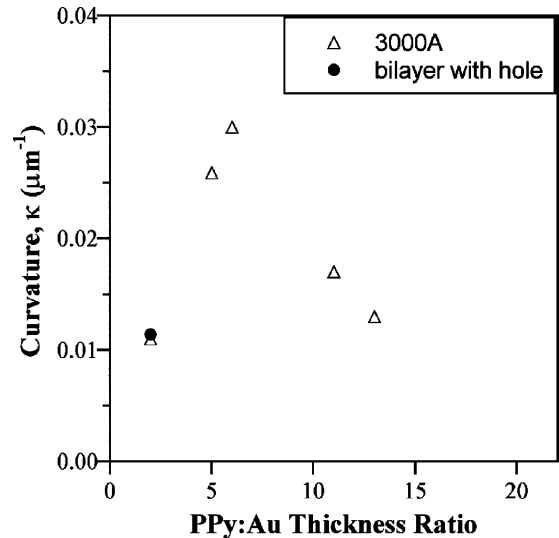
Fig. 7. Curvature of a plate-less bilayer (Au 3000 Å, PPy:Au 2:1) compared with the curvature obtained from identical bilayers with plates.

PPy:Au = 8; and $R/h = 8.4$ for Au = 0.1 μm, PPy:Au = 6). The second and third assumptions are valid as long as the strain is below the plastic deformation limit of the materials (see Section 4.3 for further discussion). The fourth assumption is true as long as the films are without defects, and measurements were only made on defect-free actuators. The validity of the fifth assumption was borne out by side-on optical microscopy images of the bilayers, by linear bending angle versus hinge length relationships (Fig. 3), and by the curvature of the plate-less bilayer devices, which all show that the bilayers bend along circular arcs.

The parameters in the model are shown in Fig. 8a: layer thicknesses h_i Young's moduli E_i, and actuation strains α_i, where i indicates the layer number, 1 for the conjugated polymer and 2 for the gold. The actuation strain α_1 is the relative change in length $\Delta l/l$ undergone by the polymer due to oxidation/reduction (redox) *when the layer is not adhered to the gold*. As discussed in Section 1, E_1 and α_1 are expected to be functions of z (making $\alpha_1(z)$ the strain at z if that incremental slice of the polymer were not in contact with any other slices). The Au layer does not experience an electrochemically induced strain, so $\alpha_2 = 0$. When an electroplated Au layer is added to the smooth Au layer
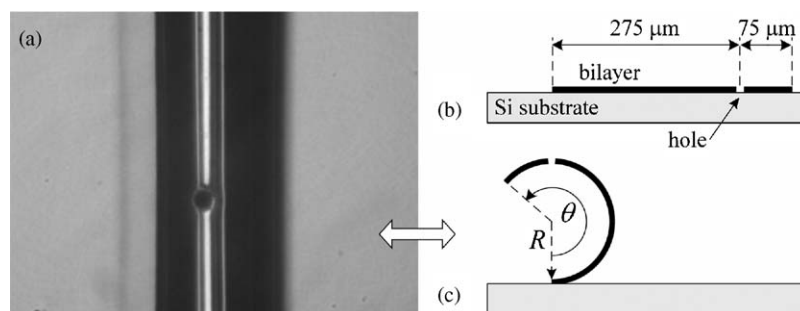
Fig. 6. (a) A curled plate-less bilayer with a hole etched through it (Au 3000 Å, PPy:Au 2:1, bilayer length 350 μm). (The top surface appears bright because it reflects light back into the microscope, while the sides reflect light away and appear dark.) Schematic side-views of (b) a flat bilayer showing the hole 275 μm from the attachment point on the substrate and (c) a curled bilayer showing the hole at the top, allowing us to obtain $R = 87.5$ μm for this actuator.
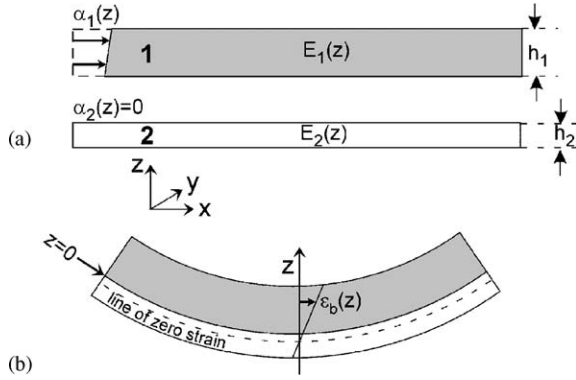
Fig. 8. (a) Actuation strain α_1 in the PPy layer 1 upon electrochemical oxidation when it is not laminated to the gold layer 2. (b) A bent bilayer, which experiences a bending strain $\varepsilon_b(z)$. The strain function $\varepsilon_b(z)$ is always linear in z and is related to the amount of bending by a purely geometric argument (see below).

to improve the adhesion of PPy [16], then E_2 is also a function of z.

As shown in Fig. 8b, *any bent bilayer* at equilibrium experiences, *by geometry*, a bending strain $\varepsilon_b(z)$ that increases linearly from the line of zero strain. Bending strain $\varepsilon_b(z)$ is the normalized difference in circumferences c at a distance z from the interface and at the interface:

$$\varepsilon_b(z) = \varepsilon_0 + \frac{c_z - c_0}{c_0} = \varepsilon_0 + \frac{2\pi(R+z) - 2\pi R}{2\pi R}$$

$$= \varepsilon_0 + \frac{z}{R} = \varepsilon_0 + \kappa z, \tag{1}$$

where ε_0 is the strain at $z = 0$, a constant that arises from defining z to be zero at the interface rather than at the line of zero strain z_0. The sign of $\varepsilon_b(z)$ changes at the line of zero strain. (The line of zero strain is found by setting $\varepsilon_b(z) = 0$, giving $z_0 = -\varepsilon_0/\kappa$; ε_0 and κ are found below.)

When a polypyrrole layer in contact with a gold layer expands or contracts due to redox, it induces bilayer curvature, which results in strains that differ from the actuation strain. In the general case, the difference between the strain imposed by geometry and the actuation strain of an unconstrained PPy layer is given by

$$\varepsilon_d^1(z) = (\varepsilon_0 + \kappa z) - \alpha_1(z), \quad z > 0, \tag{2}$$

$$\varepsilon_d^2(z) = (\varepsilon_0 + \kappa z) - \alpha_2(z), \quad z < 0, \tag{3}$$

where the superscripts refer to the layer numbers. This difference results in internal stresses σ

$$\sigma_1(z) = E_1(z)\varepsilon_d^1 = E_1(z)[(\varepsilon_0 + \kappa z) - \alpha_1(z)], \tag{4}$$

$$\sigma_2(z) = E_2(z)\varepsilon_d^2 = E_2(z)[(\varepsilon_0 + \kappa z) - \alpha_2(z)], \tag{5}$$

where the E_i may also be functions of z. The curvature at equilibrium is given by the degree of bending for which the stresses throughout the bilayer balance. When the actuators undergo free strain (no external forces applied), as they do in these bending angle studies, at equilibrium the net forces F_{net} (which translate the entire beam) and moments M_{net} (which bend the beam) must be zero

$$F_{net} = 0 = \int_{-h_2}^{h_1} \sigma(z)\,dz = \int_0^{h_1} \sigma_1(z)\,dz + \int_{-h_2}^0 \sigma_2(z)\,dz$$

$$= \int_0^{h_1} E_1(z)[(\varepsilon_0 + \kappa z) - \alpha_1(z)]\,dz$$

$$+ \int_{-h_2}^0 E_2(z)[(\varepsilon_0 + \kappa z) - \alpha_2(z)]\,dz, \tag{6}$$

$$M_{net} = 0 = \int_{-h_2}^{h_1} z\sigma(z)\,dz$$

$$= \int_0^{h_1} zE_1(z)[(\varepsilon_0 + \kappa z) - \alpha_1(z)]\,dz$$

$$+ \int_{-h_2}^0 zE_2(z)[(\varepsilon_0 + \kappa z) - \alpha_2(z)]\,dz. \tag{7}$$

Expanding and rearranging

$$\varepsilon_0 \int_0^{h_1} E_1(z)\,dz + \varepsilon_0 \int_{-h_2}^0 E_2(z)\,dz$$

$$+ \kappa \int_0^{h_1} E_1(z)z\,dz + \kappa \int_{-h_2}^0 E_2(z)z\,dz$$

$$= \int_0^{h_1} E_1(z)\alpha_1(z)\,dz + \int_{-h_2}^0 E_2(z)\alpha_2(z)\,dz,$$

$$\varepsilon_0 \int_0^{h_1} zE_1(z)\,dz + \varepsilon_0 \int_{-h_2}^0 zE_2(z)\,dz$$

$$+ \kappa \int_0^{h_1} E_1(z)z^2\,dz + \kappa \int_{-h_2}^0 E_2(z)z^2\,dz$$

$$= \int_0^{h_1} zE_1(z)\alpha_1(z)\,dz + \int_{-h_2}^0 zE_2(z)\alpha_2(z)\,dz, \tag{8}$$

and writing in matrix form

$$\begin{bmatrix} \int_0^{h_1} E_1(z)\,dz + \int_{-h_2}^0 E_2(z)\,dz & \int_0^{h_1} E_1(z)z\,dz + \kappa \int_{-h_2}^0 E_2(z)z\,dz \\ \int_0^{h_1} zE_1(z)\,dz + \int_{-h_2}^0 zE_2(z)\,dz & \int_0^{h_1} E_1(z)z^2\,dz + \int_{-h_2}^0 E_2(z)z^2\,dz \end{bmatrix} \begin{bmatrix} \varepsilon_0 \\ \kappa \end{bmatrix} = \begin{bmatrix} \int_0^{h_1} E_1(z)\alpha_1(z)\,dz + \int_{-h_2}^0 E_2(z)\alpha_2(z)\,dz \\ \int_0^{h_1} zE_1(z)\alpha_1(z)\,dz + \int_{-h_2}^0 zE_2(z)\alpha_2(z)\,dz \end{bmatrix}. \tag{9}$$

These two equations in the two unknowns ε_0 and κ can be solved simultaneously. Representing the left-hand matrix as A and the right-hand matrix as B,

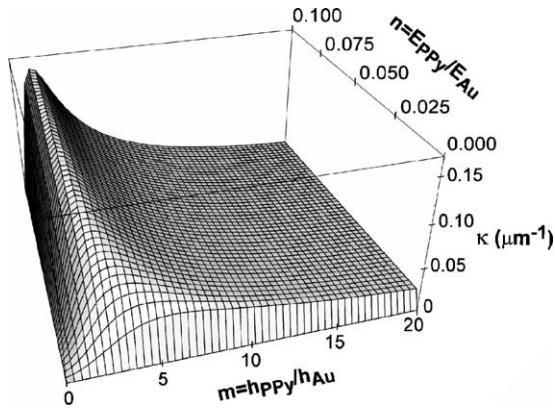$$\begin{bmatrix} \varepsilon_0 \\ \kappa \end{bmatrix} = A^{-1}B. \tag{10}$$

Fig. 9. Curvature as a function of thickness ratio $m = h_1/h_2$ and Young's modulus ratio $n = E_1/E_2$ according to Equation (11) ($\alpha_1 = 3\%$, $\alpha_2 = 0$, $h_2 = 0.1\ \mu m$).

We used Mathematica to perform these calculations. (The code is available from the authors upon request.)

4.2. Curvature

When the E_i and α_i are constant, the curvature expression reduces to the Timoshenko equation [8]

$$\frac{1}{R} = \kappa = \frac{\alpha_1 - \alpha_2}{h_2} \frac{6mn(1 + m)}{1 + 4mn + 6m^2n + 4m^3n + m^4n^2}, \quad (11)$$

where $m = h_1/h_2$ and $n = E_1/E_2$. The Timoshenko equation was developed in the context of actuation strain due to thermal expansion, but it is a general formulation that can be used for bilayer bending arising from other types of strain.

Fig. 9 shows the curvature as a function of m and n predicted by Equation (11) for $\alpha_1 = 3\%$, $\alpha_2 = 0$, and $h_2 = 0.1\ \mu m$. (For convenience, α_1 is given as a positive number and κ is displayed as positive, although the PPy actually contracts. This does not affect any of the calculated magnitudes.) There is a peak in curvature along the thickness ratio axis m that results from a trade-off between increasing the force by adding PPy and increasing the difficulty of bending by making the beam thicker. As the Young's modulus of the PPy increases relative to the Au (increasing n),

the peak becomes narrower and higher, and it shifts to smaller thickness ratios.

Fig. 10 shows cross-sections through Fig. 9 at constant n using literature estimates of α_1, E_1, and E_2. Inplane strain in PPy(DBS) has been measured to be 0.35–3.6% [11,17], and the modulus of PPy(DBS) has been reported to be 0.15–0.25 GPa in the reduced state (flat) and 0.45 GPa in the oxidized state (bent) [17]. The bulk modulus of gold is 83 GPa, but for thin gold films it is lower, with reported values from 78 GPa [18] down to 53 GPa [19]. Using values of 3%, 0.4 GPa, and 83 GPa resulted in the solid line curves, taken to be a base case, which has a peak at a PPy:Au thickness ratio $m = 4.25$. Note that since the moduli appear in Equation (11) only as a ratio, changing the moduli to $E_1 = 0.26$ and $E_2 = 54$ GPa gives exactly the same base curve. Changing the strain (Fig. 10a) results in a linear change in peak height, as is evident from the equation, but no change in peak position. Increasing the PPy modulus to bring it closer to that of Au (Fig. 10b), or decreasing the Au modulus to bring it closer to that of PPy (Fig. 10c), results in sharpening the peak and moving it leftward, as shown in Fig. 9, as well as increasing the peak height.

In Fig. 10, the Au thickness was held fixed. If one were to hold the PPy:Au thickness ratio constant and vary the total bilayer thickness $h = h_1 + h_2 = (m + 1)h_2$, then curvature would increase steeply as h was decreased, since κ is proportional to $1/h_2$ in Equation (11).

Since it is known that the PPy bends by itself when it delaminates from the Au, there must be either a strain gradient or a modulus gradient, or both, in the film. As discussed above, this can be hypothesized to arise from continued crosslinking and/or degradation of the chains throughout electrochemical deposition, which would result in reduced electroactivity and lower strain at the electrode surface in comparison with the electrolyte surface. There may also be accompanying changes in modulus. Since thickness is linearly proportional to deposition time for thin films, we can write expressions for strain decreasing with time/thickness and modulus increasing with time/thickness. We chose exponentially decreasing functions that describe the declining probability of forming a new crosslink or defect over
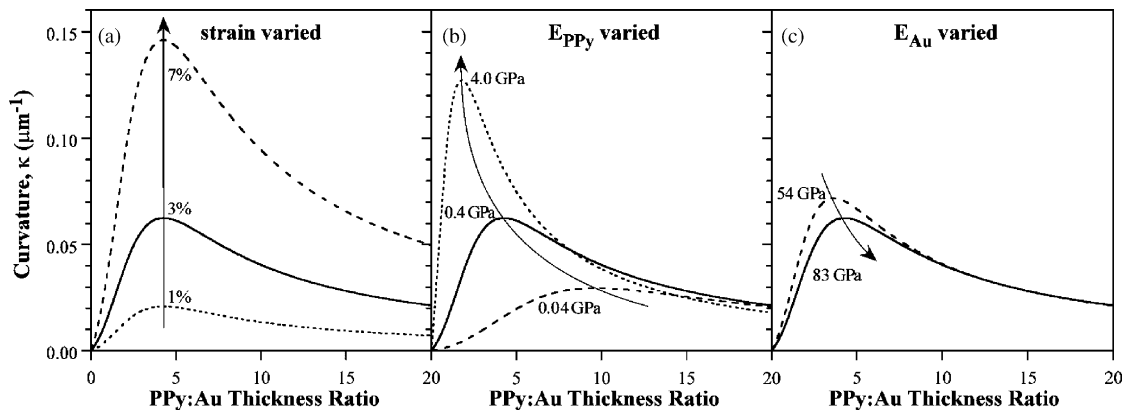

Fig. 10. Curvature predicted by the Timoshenko Equation (11) as a function of PPy:Au thickness ratio m for a gold thickness h_2 of 1000 Å. The solid lines represent the base case with a strain of 3%, PPy modulus E_2 of 0.4 GPa, and Au modulus E_1 of 83 GPa. Curvature upon varying the (a) strain, (b) PPy modulus, and (c) Au modulus around the base case, with arrows indicating increasing size of the parameter.
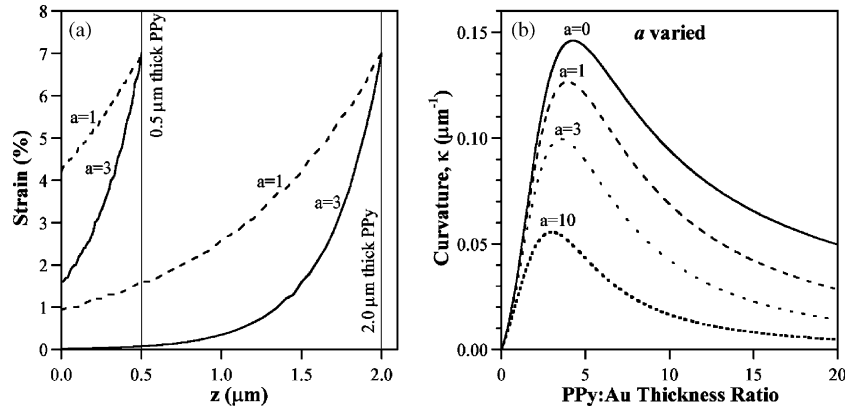
Fig. 11. (a) Strain dependence given by Equation (12) as a function of distance z from the metal interface for two different film thicknesses and values of a. (b) Curvature as a function of PPy:Au thickness ratio m for different values of a ($\alpha_b = 0\%$, $\alpha_0 = 7\%$, $h_2 = 0.1$ μm, $E_1 = 0.4$ GPa, $E_2 = 83$ GPa).

time as available sites are consumed, so that the loss in actuation or increase in modulus gradually slows. Such functions go smoothly from the surface to the bulk values and are consistent with our understanding of the chemical processes occurring in the film. (Linear functions would be inappropriate, for example, because they go to negative values with increasing h_1.)

$$\alpha_1(z) = \alpha_b + \alpha_0\, e^{-a(h_1-z)}, \tag{12}$$

$$\begin{aligned} E_1(z) &= E_0(c_1 - c_2\, e^{-a(h_1-z)}) \\ &= E_0(c_1 - (c_1-1)\, e^{-a(h_1-z)}). \end{aligned} \tag{13}$$

Here α_b is the actuation strain in the bulk material, $\alpha_b + \alpha_0$ and E_0 are the strain and modulus in freshly-deposited material at the outer PPy surface, respectively, and we set $c_2 = c_1 - 1$. Fig. 11a illustrates the strain of Equation (12) for two film thicknesses and values of a with $\alpha_b = 0$. (A non-zero α_b simply introduces a vertical offset to the curves.)

Solving Equation (9) with the strain dependence in (12) and constant E_1 gives

$$\kappa = \frac{\left(6\alpha_0\, e^{-ah_2 m}\, n\left\{[2 + 2mn + ah_2(-1 + m^2 n) + e^{ah_2 m}(-2(1 + mn) + ah_2(1 + 2m + m^2 n))] + a^2\frac{\alpha_b}{\alpha_0}\, e^{ah_2 m}\, h_2^2 m(1 + m)\right\}\right)}{a^2 h_2^3[1 + 4mn + 6m^2 n + 4m^3 n + m^4 n^2]}. \tag{14}$$

The curvatures for this case are shown in Fig. 11b for different values of a, a strain at the surface α_0 of 7%, and the remaining parameters the same as the base case of Fig. 10. The steeper the gradient, the smaller the curvature: since α_0 sets the value at the surface, a larger a means a smaller strain throughout the rest of the film. The peak also becomes sharper and moves leftward.

Solving Equation (9) with the modulus dependence as in (13) and constant α_1 gives

The curvatures are shown in Fig. 12 for different values of a and c_1, with the remaining parameters the same as the base case of Fig. 10. Raising these numbers causes the peak to become higher and sharper (as the modulus at the interface gets closer to that of the Au), and to shift leftward, but the tail at higher m does not change. Fig. 12c shows how the curvature decreases with total beam thickness.

4.3. Bending strain

When the E_i and α_i are constant, the strain at the PPy/Au interface ($z = 0$) is given by

$$\varepsilon_0 = (\alpha_1 - \alpha_2)\frac{mn(4 + 3m + m^3 n)}{1 + 4mn + 6m^2 n + 4m^3 n + m^4 n^2}. \tag{16}$$

Fig. 13a shows ε_0 as a function of m for literature values of the parameters for PPy and Au. The maximum strain at the interface occurs at the same m as the maximum curvature, which for the values used in this example are 4.25.

While the strain across the PPy/Au interface is continuous by geometry, the stress is not. The stress is given by the difference between the bending and free actuation strains multiplied by the Young's modulus (Equations (4) and (5)). The interfacial stress σ_0 is given by the difference in stress in the polymer just above the interface, at $z = 0^+$, and in the gold just below the interface,

$$\kappa = \frac{n\alpha_1 6a^2\, e^{ah_2 m}\, h_2\{2 - ah_2 + e^{ah_2 m}(-2 + ah_2 + 2ah_2 m) + c_1[-2 + ah_2 + e^{ah_2 m}(2 + a^2 h_2^2 m(1 + m) - a(h_2 + 2h_2 m))]\}}{\{12(-1 + c_1)^2(-1 + e^{ah_2 m})^2 n^2 - 24a(-1 + c_1)\, e^{ah_2 m}(-1 + e^{ah_2 m})h_2 n(1 + c_1 mn) }.$$
$$+ a^4\, e^{2ah_2 m}\, h_2^4[1 + 2c_1 m(2 + 3m + 2m^2)n + c_1^2 m^4 n^2] + 12a^2(-1 + c_1)\, e^{ah_2 m}\, h_2^2 n[-1 + m^2 n + e^{ah_2 m}(1 + 2m + c_1 m^2 n)]$$
$$-4a^3(-1 + c_1)\, e^{ah_2 m}\, h_2^3 n[-1 - c_1 m^3 n + e^{ah_2 m}(1 + 3m + 3m^2 + c_1 m^3 n)]\}$$
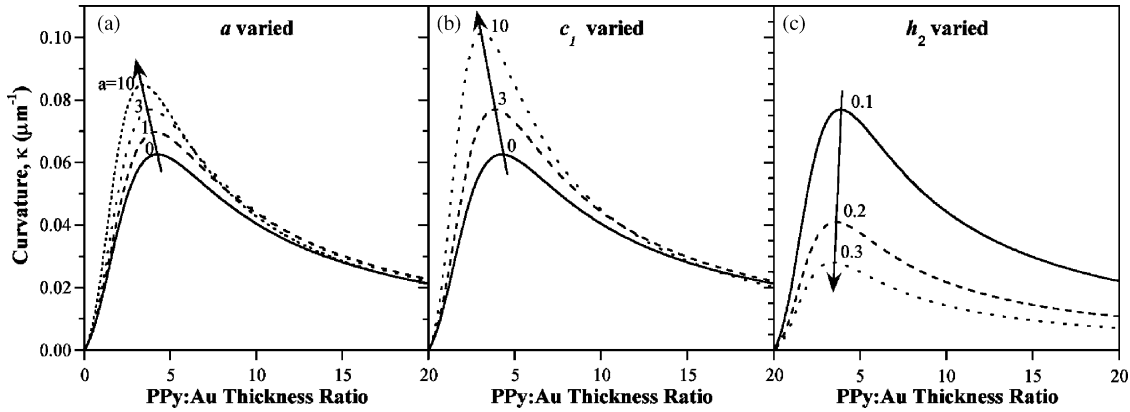$$\tag{15}$$

Fig. 12. Curvature as a function of PPy:Au thickness ratio m with the modulus dependence given by Equation (13). The effect of varying (a) a, (b) c_1, and (c) h_2 ($\alpha_1 = 3\%$, $E_0 = 0.4$ GPa, $E_2 = 83$ GPa, $c_2 = c_1 - 1$, and, unless varied, $a = 3$, $c_1 = 3$, and $h_2 = 0.1$ μm).

at $z = 0$:

$$\sigma_0 = \sigma_1(0^+) - \sigma_2(0^-) = E_1(\varepsilon_1(0^+) - \alpha) - E_2\varepsilon_2(0^-)$$

$$= \varepsilon_0(E_1 - E_2) - E_1\alpha. \tag{17}$$

Interfacial stress is the cause of delamination. Since E_{PPy} and E_{Au} differ by 2 orders of magnitude, and since actuators are fabricated with the ratio that gives maximum curvature (to save chip real estate), the stress is substantial, on the order of 4 MPa for a strain of 5%. (Interfacial stress can be eliminated without sacrificing performance by introducing a strain-less but electrically conducting "buffer layer" [20].)

The bending-induced strain at other places in the bilayer, $\varepsilon_b(z)$, is found using Equation (1). As the PPy contracts, the outer surface of the Au (at $z = -h_2$) undergoes tensile strain (stretching, indicated by values less than 0 for consistency with the previous section) until approximately $m = 30$. Thereafter, the PPy is so thick that there is little bending and the whole bilayer contracts, putting the Au film under compression. For these parameters, the maximum tensile strain reached in the Au is very close to the value at which it starts to plastically deform, which is ~0.3% for thin films [19]. Above this value, the stress–strain curve is no longer linear, violating the model assumptions. Therefore, ε_b should be checked for case-specific bilayer parameters.

There has been some confusion in the literature regarding strain in bending actuators, with some groups reporting the geometric bending strain at the PPy surface as the actuation strain. As shown in Fig. 13b, the strain at the outer surface of the PPy ($h_1 = mh_2$) depends strongly on m. For small values of m, the bending strain at h_1 is much smaller than the actuation strain, but at the peak m it can attain larger values than α_1, in this example 4.3% compared to 3%. This illustrates the importance of not confusing actuation strain, a material property, with bending strain, a geometry-dependent quantity. It should also be noted that, for the parameters used in this example, the peak stress $\sigma_{p1} = \varepsilon_b(z = h_1)E_1 = 0.043 \times 0.4$ GPa = 17 MPa, which exceeds the 11–15 MPa ultimate tensile strength of PPy(DBS) [17].

The line of zero strain, z_0 starts two thirds of the way into the Au film at $m = 0$ and approaches $z = 0$ with increasing m until $m = 4.25$ (Fig. 14a). The line of zero strain then reverses direction and heads back toward the outer Au surface, leaving the film for $m > 25$. Fig. 14b shows why this is the case, plotting strain versus position in a bilayer with gold thickness $h_2 = 0.1$ μm and PPy thicknesses $h_1 = 0.1$, 0.425, 1.5, and 4 μm ($m = 1$, 4.25, 15, and 40). For $m = 1$, the strain is zero at $z = -0.067$ μm; to the left of that the Au is in tension, and to the right it is in compression. For $m = 4.25$, z_0 has moved towards the PPy interface slightly and the slope is greater. As m increases above that, the slope drops and the line pivots, so that by $m = 40$, the gold is entirely in com-
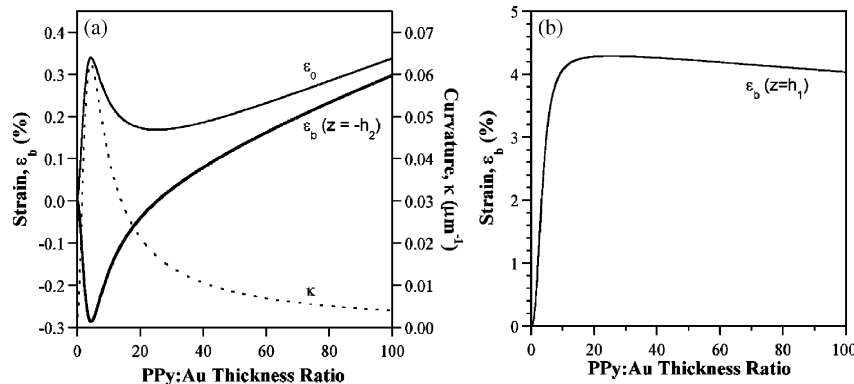

Fig. 13. (a) Strain ε_0 at the PPy/Au interface and $\varepsilon_b(z = -h_2)$ at the outer Au surface versus PPy:Au thickness ratio m, with curvature shown for comparison. (b) Strain $\varepsilon_b(z = h_1)$ at the outer PPy surface versus m. All strains asymptote to α_1, and κ tends toward 0, as $m \to \infty$ ($\alpha_1 = 3\%$, $h_2 = 0.1$ μm, $E_1 = 0.4$ GPa, $E_2 = 83$ GPa).
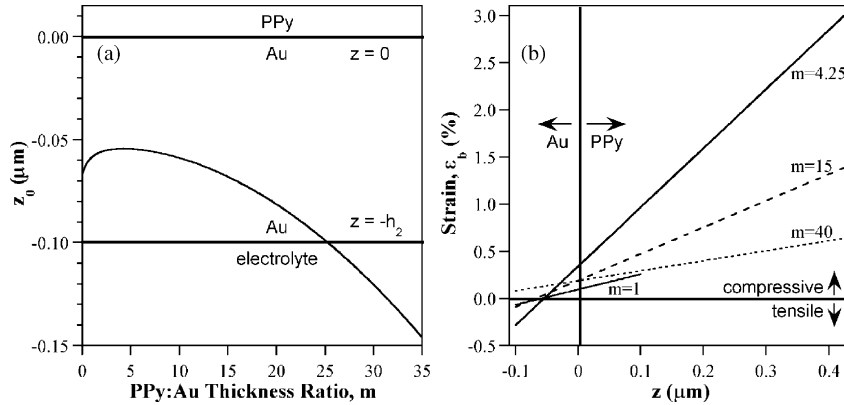
Fig. 14. (a) Position of the line of zero strain z_0, which starts in the Au layer, as a function of m. The interfaces of the Au are indicated. (b) Strain as a function of z for PPy layers of different thickness, with m indicated in the figure as well as the Au/PPy interface (note that panel (a) has a vertical z-axis, while in panel (b) the z-axis is horizontal) ($\alpha_1 = 3\%$, $h_2 = 0.1\,\mu m$, $E_1 = 0.4\,GPa$, $E_2 = 83\,GPa$).

pression. Thus, the strain everywhere in the bilayer approaches the actuation strain α_1 as $m \to \infty$, and κ goes to zero.

5. Comparison of model with experiment

5.1. Constant strain

The experimental data are compared with the Timoshenko equation prediction (constant strain and modulus for all cases, Equation (11)) in Fig. 15. The equation has two adjustable parameters: n (the moduli of the PPy and Au only come into the equation as a ratio) and α_1. Published values for the modulus of thin films of gold are smaller than the bulk value of 83 GPa, but the values for our gold films were unknown. We therefore used 83 GPa, with the understanding that the modulus values found for the PPy may actually be somewhat smaller if this gold modulus is too high.

The PPy strain and modulus values for the model were chosen to obtain a reasonable match to the $h_2 = 0.1\,\mu m$ data set, and

the other curves were generated using the same numbers. This approach under-predicted the peak height for $h_2 = 0.05\,\mu m$ and over-predicted the heights for $h_2 = 0.2$ and $0.3\,\mu m$. The data were fit more successfully if different strains were used for each curve, with higher strains for bilayers having thinner gold layers. This is consistent with the presence of a strain gradient within the film.

5.2. Strain gradient

The model that included the strain variation given in Equation (12) is compared with the experimental data in Fig. 16. This model had three parameters that were adjusted: n (through E_1), α_0, and a. Broadly speaking, the m-position of the peak was determined by E_1, α_0 was adjusted to match the peak height of the $h_2 = 0.1\,\mu m$ data set, and a determined the relative heights for the other Au thicknesses. The parameters are not completely independent, however. The value of E_1 also affects peak height and thus α_0, and once E_1 is chosen, only a single value of a
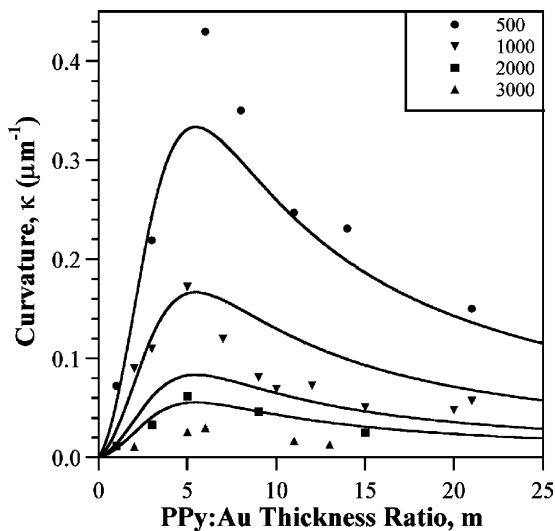

Fig. 15. Comparison of Timoshenko equation values (lines) with the experimental data of Fig. 4 (points) for a constant strain $\alpha_1 = 10\%$ and constant moduli $E_1 = 0.2\,GPa$, $E_2 = 83\,GPa$. Using the Timoshenko model (Equation (11)), the data cannot all be fit, no matter what parameters are chosen.
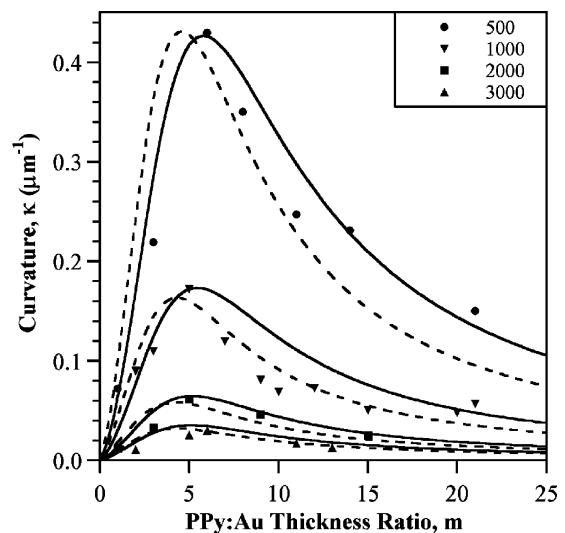
Fig. 16. Comparison of data with a model using the strain of Equation (12) with fixed $\alpha_b = 3\%$ and $E_2 = 83\,GPa$ from the literature, and fitting to obtain (solid lines) $\alpha_0 = 17\%$, $a = 3.4$, and $E_1 = 0.12\,GPa$ and (dashed lines) $\alpha_0 = 17\%$, $a = 7$, and $E_1 = 0.2\,GPa$.

produces the correct relative heights of the four curves. The bulk actuation strain was fixed at $\alpha_b = 3\%$ since Bay et al. [17] reported strains of 2.5–3.5% for 10 μm thick PPy films doped with different dodecylbenzene sulfonates. (Commercial DBS contains a mixture of alkyl chain lengths and attachment positions [3].)

Two sets of curves are shown in Fig. 16. Both have $\alpha_0 = 17\%$, but the solid lines use $a = 3.4$ and $E_1 = 0.12$ GPa, while the dashed lines use $a = 7$ and $E_1 = 0.2$ GPa. (If $E_{Au} = 54$ GPa instead of 83 GPa, then the values of E_1 would be 0.08 and 0.13 GPa, respectively). The former better fit the data at large m and the positions of the peaks for the thicker gold films, while the increased sharpness of the latter provided a slightly better fit near the peak maximum. (Fig. 3 in the Supplementary Data shows the strain as a function of position in the film for these values, and is analogous to Fig. 11a, which used arbitrary example values.)

This 20% strain ($\alpha_0 + \alpha_b$) at the outer PPy surface is significantly larger than expected, and the strain gradients are substantial. For a PPy thickness $h_1 = 2.0$ μm, the strain at the PPy/Au interface is already reduced to the bulk 3%.

This model was clearly more successful than the Timoshenko equation in capturing the principal bending behaviors of all four sets of curvature data with a single set of numbers E_1, α_0, and a. However, the model did not capture all of the complexity: no adjustments of the model parameters were able to produce perfect fits to all four curves. The solid and dashed curves fit different aspects of the data better.

We hypothesize that the model failed to fully account for the data because model assumption 3 was violated. With a strain variation in the film of the form of Equation (12), the expression for ε_0 becomes

$$\varepsilon_0 = \frac{\left(\begin{array}{l} \alpha_0\, e^{-ah_2 m}\, n\left\{ -2[-3 + 3m^2 n + 2a(h_2 + h_2 m^3 n) \right. \\ \left. + e^{ah_2 m}[3 - 3m^2 n + ah_2(-2 - 3m + m^3 n)]] \right. \\ \left. + \frac{\alpha_b}{\alpha_0} a^2 h_2^2\, e^{ah_2 m}\, m(4 + 3m + m^3 n)\right\} \end{array}\right)}{a^2 h_2^2[1 + 4mn + 6m^2 n + 4m^3 n + m^4 n^2]}.$$

(18)

The strain $\varepsilon_b(z)$ was found by combining Equations (1), (14), and (18). The strain at the outer edge of the gold film and the stress at the outer edge of the PPy film are shown in Fig. 17, together with horizontal lines indicating reported values of the elastic limit and ultimate strain for Au films 0.3 μm thick [19] and the ultimate tensile strength (UTS) for PPy(DBS) films 10 μm thick [17]. The elastic limit and ultimate strain of Au thin films are strongly dependent on thickness and dimensions [19], so these lines represent only approximate values for our devices. The UTS for the PPy may likewise be different in our thinner films.

During actuation, Fig. 17 indicates that the gold is likely to be plastically deformed in many of our devices, and for those with the greatest bending, it may rupture. In addition, for the actuators with greatest bending it is also possible that the PPy is plastically deformed or that its UTS is exceeded. However, SEM images of actuators with 0.05 μm Au and $m = 6$ did not reveal any cracks. Plastic deformation would occur only during the initial actuation cycles, after which the gold would be stretched and thinned and possibly strain-hardened to a higher modulus, and would no longer be driven outside the elastic limit.

5.3. Modulus gradient

The m-position of the peaks is determined primarily by the Young's modulus. The modulus of 0.12–0.20 GPa for the oxidized state from the model fit is lower than the 0.45 GPa previously reported for 10 μm thick PPy(DBS) films [17]. Since the peak shifted to slightly higher values of m with increasing PPy thickness, the films behaved as if they became softer with thickness, retreating from, rather than approaching, the bulk value. This led us to investigate whether there might be a modulus gradient in the film, increasing from a small thin-film value to the larger thick-film value. In addition, Figs. 10 and 12 show that a change in modulus can produce sharper peaks, needed to better match the data.

The data were compared with a model that included a modulus variation of the form in Equation (13). This model was clearly inconsistent with the data (the Supplementary Data includes a figure showing this). A modulus gradient in the opposite direc-
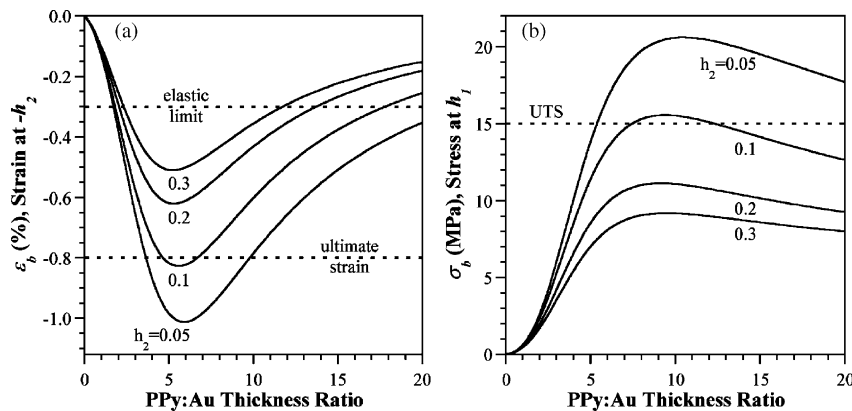

Fig. 17. For the parameters of the solid lines in Fig. 16: (a) the strain at the outer surface of the gold film for the four different Au thicknesses, compared with the approximate elastic limit and ultimate strain of 0.3 μm thick Au films and (b) the stress at the outer surface of the PPy film compared with the ultimate tensile strength of 10 μm thick PPy(DBS). The horizontal lines are dashed to indicate that these values may not be valid for our devices.

tion, lower at the gold interface and higher at the surface of the PPy, comparable to Equation (12), was also tested, and was likewise inappropriate: although it accounted for the right-ward shift of the peak positions, the peaks from this model were too broad. Adding a modulus gradient to the strain gradient of Section 5.2 also degraded, rather than improved, the fit.

We therefore conclude that there is no significant modulus gradient corresponding to the strain gradient in the film. These results also show that the good fit for the model with variable strain was not simply a result of having enough parameters in the model: adding more parameters subjected to realistic physical constraints did not improve the fit, but instead worsened it.

6. Model validation

In order to validate the model, independent experiments were performed to obtain the Young's modulus and the strain gradient. The former measurements are described in detail in Part 2 of this series, but in summary a stress–strain curve was obtained for the bilayer (a force transducer measured the force exerted by a bent bilayer as the transducer z-position was changed), and the modulus was found by comparing the data with a bending beam model. The modulus in the oxidized state was found to be 0.2 GPa for a 1.9 μm thick PPy film, assuming that $E_{Au} = 83$ GPa, in reasonable agreement, given the uncertainties involved in the measurements, with the values of 0.12–0.20 GPa obtained using our varying strain model. (If $E_{Au} = 54$ GPa, then $E_{PPy} = 0.13$ GPa, compared with 0.08–0.13 GPa from the varying strain model.)

To independently determine the magnitude of the strain gradient, the gold was removed from the back of a set of bilayers with 0.1 μm Au and $m = 19$ ($h_1 = 1.92$ μm). These samples had previously been electrochemically cycled, but were unlikely to have undergone strains outside the elastic regime (Fig. 17). The actuators were immersed in gold etchant for 90 s, resulting in PPy films attached to SU8 plates, but with no Au backing (Fig. 18). Where the PPy/Au was not released from the surface, the etchant did not remove the gold, so the electrical connections to the base of the free PPy layer were preserved. Data were taken from four actuators with hinge lengths from 10 to 30 μm.
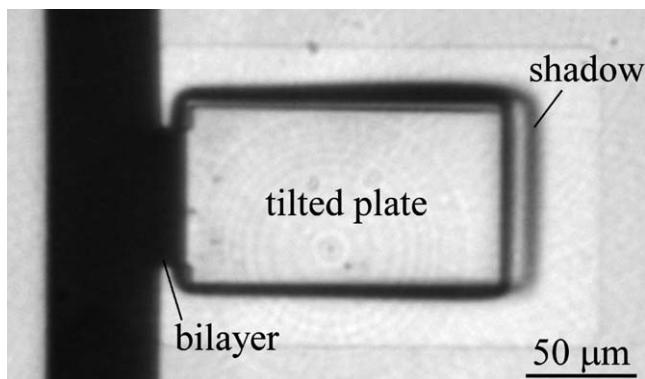

Fig. 18. Actuator in the oxidized (bent) state after Au was removed from the back, leaving the plates transparent. (The differential adhesion region around the actuator can be seen surrounding the plate.)

In the oxidized state, the PPy layer had a curvature of $\kappa = 0.0271 \pm 0.0009$ μm^{-1} ($R = 36.9$ μm), confirming the existence of the strain gradient. The curvature decreased upon application of -1 V versus Ag/AgCl, but the PPy remained partially bent because it could not be completely reduced without the gold backing in the presence of oxygen [21].

The bilayer model with a varying strain was modified by setting the gold thickness to zero, giving

$$\kappa = \frac{6\alpha_0 \, e^{-ah_1}(2 + ah_1 + e^{ah_1}(-2 + ah_1))}{a^2 h_1^3}. \tag{19}$$

Note that the parameter a has units of μm^{-1}.

Inserting $h_1 = 1.92$ μm and using the strain values from the dashed lines in Fig. 16, $\alpha_0 = 17\%$, $\alpha_b = 3\%$, and $a = 7$, gave a curvature of 0.0336 μm^{-1} ($R = 29.7$ μm). This is also rather good agreement given the experimental uncertainties. (Gold etchant contains KI and I$_2$, and while it has not been observed to be detrimental to PPy, its effect is unknown.)

7. Discussion and conclusions

Curvature when bilayers undergo free strain (no external loads) depends on the actuation strain, the total thickness of the bilayer, the ratio of the PPy to Au thicknesses, and the ratio of their Young's moduli. The strain at the outer surfaces of the bent beam can be much larger or smaller than the actuation strain.

The PPy(DBS) microfabricated bilayers straightened to within a few degrees of completely flat upon reduction, and bent upon oxidation to angles that depended linearly on hinge length (until θ exceeded 180°), showing that the hinges formed perfect circles. The optimum thickness ratio of PPy(DBS) to Au was ~5:1, and this shifted only slightly with total bilayer thickness. At this ratio, a radius of curvature of 2 μm was achieved with an Au layer of 500 Å. Further increases in curvature are possible by scaling down film thicknesses and by using higher-resolution masks and microfabrication equipment. A layer of electroplated Au added to improve adhesion behaved mechanically as if it were a solid film of approximately half the measured thickness.

The Timoshenko bilayer equation with literature values for the strain and modulus predicted bending angles that were of the right order of magnitude. Using a single set of modulus and strain values, however, it did not correctly account for the change in peak height as the gold thickness was varied for constant PPy:Au ratios: the data were spread out more widely than the simple predicted dependence of $1/h_2$. To capture the basic behavior of all the data sets, it was necessary to add a strain gradient to the model, with bulk values of strain at the gold interface but higher strains at the outer PPy surface. Such a gradient had been expected from prior observations reported in the literature. With this approach, all the data could be fit with a single set of parameters. These model prediction parameter values were verified in separate experiments.

It is clear that a range of thickness ratios and several Au thicknesses are needed to distinguish between competing models if the strain or modulus are z-dependent. While bulk values provide a starting point for estimating thin film values, they can

vary significantly for reasons that are still not fully understood. For PPy(DBS), the average actuation strain for the thinnest films was ∼20%, while for thicker films it was closer to 3%. Likewise, the thin film oxidized-state modulus was only 0.12–0.20 GPa, compared with bulk values of 0.45 GPa.

It would have been reasonable to assume that a modulus gradient co-existed with the strain gradient, since a loss of strain is associated with a loss of electroactivity, which is in turn related to chain defects such as crosslinks. However, our modeling indicated that only the strain has a significant non-uniformity in the z-direction in the PPy. The constant modulus suggests that the electronic defects may arise primarily from substituents, such as hydroxyl and carbonyl groups, which have been observed in cases of over-oxidation [22,23].

The actuation strain and Young's modulus of thin PPy(DBS) films are now known, but if PPy is produced with a different dopant or under different deposition conditions, then this material would be expected to have different properties, and it would need to be characterized in a like manner. For system design, force and speed data are also needed, and these metrics are taken up in the next two papers of this series.

Acknowledgements

Appendix A. Supplementary data

Supplementary data associated with this article can be found, in the online version, at 10.1016/j.snb.2005.10.023.

References

[1] D. Leo, E. Smela, J. Madden, K. Kim, Z. Ounaies, D.F. Infante, Standard testing methods for extensional and bending electroactive polymer actuators, Proceedings of the ASME 2005, International Mechanical Engineering Congress and Exposition (IMECE), Orlando, FL, November 5–11, p. 2005-82440, submitted for publication.

[2] E. Smela, Conjugated polymer actuators for biomedical applications, Adv. Mater. 15 (6) (2003) 481–494.

[3] E. Smela, Microfabrication of PPy microactuators and other conjugated polymer devices, J. Micromech. Microeng. 9 (1999) 1–18.

[4] E. Smela, N. Gadegaard, Volume change in polypyrrole studied by atomic force microscopy, J. Phys. Chem. B 105 (39) (2001) 9395–9405.

[5] T.F. Otero, H.-J. Grande, J. Rodriguez, Reinterpretation of polypyrrole electrochemistry after consideration of conformational relaxation processes, J. Phys. Chem. B 101 (1997) 3688–3697.

[6] T.F. Otero, H. Grande, J. Rodriguez, Role of conformational relaxation on the voltammetric behavior of polypyrrole. Experiments and mathematical model, J. Phys. Chem. B 101 (1997) 8525–8533.

[7] T.F. Otero, J. Padilla, Anodic shrinking and compaction of polypyrrole blend: electrochemical reduction under conformational relaxation kinetic control, J. Electroanal. Chem. 561 (1) (2004) 167–171.

[8] S. Timoshenko, Analysis of bi-metal thermostats, J. Opt. Soc. Am. 11 (1925) 233–256.

[9] Q. Pei, O. Inganäs, Electrochemical applications of the bending beam method. 1. Mass transport and volume changes in polypyrrole during redox, J. Phys. Chem. 96 (1992) 10507–10514.

[10] Q. Pei, O. Inganäs, Electrochemical applications of the bending beam method. 2. Electroshrinking and slow relaxation in polypyrrole, J. Phys. Chem. 97 (1993) 6034–6041.

[11] Q. Pei, O. Inganäs, Electrochemical applications of the bending beam method; a novel way to study ion transport in electroactive polymers, Solid State Ionics 60 (1993) 161–166.

[12] E. Smela, M. Kallenbach, J. Holdenried, Electrochemically driven polypyrrole bilayers for moving and positioning bulk micromachined silicon plates, J. Microelectromech. Syst. 8 (4) (1999) 373–383.

[13] K. Naoi, Y. Oura, M. Maeda, S. Nakamura, Electrochemistry of surfactant-doped polypyrrole film(I)—formation of columnar structure by electropolymerization, J. Electrochem. Soc. 142 (2) (1995) 417.

[14] J.C. Hooker, I. Johanssen, E. Smela, Monitoring volume expansion in PPy(DBS) with AFM: effects of DBS isomers, Annual Report, Risø National Laboratory, Roskilde, Denmark, 1999.

[15] Y. Liu, Q. Gan, S. Baig, E. Smela, Improving adhesion of polypyrrole to gold for long-term actuation, in: Y. Bar-Cohen (Ed.), Proceedings of the SPIE's 12th Annual International Symposium on Smart Structures and Materials, March 6–10, Electroactive Polymer Actuators and Devices (EAPAD), San Diego, CA, 2005.

[16] M. Pyo, C.C. Bohn, E. Smela, J.R. Reynolds, A.B. Brennan, Direct strain measurement of polypyrrole actuators controlled by the polymer/gold interface, Chem. Mater. 15 (4) (2003) 916–922.

[17] L. Bay, N. Mogensen, S. Skaarup, P. Sommer-Larsen, M. Jorgensen, K. West, Polypyrrole doped with alkyl benzenesulfonates, Macromolecules 35 (25) (2002) 9345–9351.

[18] V.K. Pamula, A. Jog, R.B. Fair, Mechanical property measurement of thin-film gold using thermally actuated bimetallic cantilever beams, in: Nanotech 2001, Tech. Proc. Int. Conf. Modeling and Simulation of Microsystems, vol. 1, 2001, pp. 410–413 (Chapter 8).

[19] H.D. Espinosa, B.C. Prorok, Size effects on the mechanical behavior of gold thin films, J. Mater. Sci. 38 (2003) 4125–4128.

[20] B. Shapiro, E. Smela, Bending actuators with maximum curvature and force and zero interfacial stress, J. Intell. Mater. Syst. Struct., in press.

[21] L. Bay, K. West, N. Vlachopoulos, S. Skaarup, Potential profile in a conducting polymer strip, in: Y. Bar-Cohen (Ed.), Proceedings of the SPIE's Eighth International Symposium on Smart Structures and Materials, vol. 4329, March 5–8, Electroactive Polymer Actuators and Devices (EAPAD), Newport Beach, CA, 2001, pp. 54–58.

[22] J.B. Schlenoff, H. Xu, Evolution of physical and electrochemical properties of polypyrrole during extended oxidation, J. Electrochem. Soc. 139 (9) (1992) 2397.

[23] J. Lei, C.R. Martin, Infrared investigations of pristine polypyrrole—Is the polymer called polypyrrole really poly(pyrrole-co-hydroxypyrrole)? Synth. Met. 48 (1992) 331.

Biographies

Marc Christophersen received his MS and PhD in Materials Science from the University of Kiel, Germany, in 1998 and 2002, respectively. From 2002 to 2003 he was a postdoctoral fellow at the University of Rochester in Dr. Fauchet's group. He worked at Lake Shore Cryotronics, Inc. from 2003 to 2004 as a senior scientist for electrochemistry. Since 2004, he has been at the Department of Mechanical Engineering, University of Maryland as a postdoctoral fellow working on electroactive polymers for MEMS applications.

Benjamin Shapiro completed his BS at Georgia Tech in 1995 and received his PhD from Caltech in the Control and Dynamical Systems option in 1999. He is an assistant professor in the Aerospace Department at the University of Maryland. His interests include modeling, design, and control of micro-scale systems.

Elisabeth Smela received her BS from MIT in physics in 1985 and PhD from the University of Pennsylvania in electrical engineering in 1992. She is an associate professor in the Department of Mechanical Engineering at the University of Maryland. Current fields of interest include polymer MEMS and bio-MEMS/μITAS.